Carbohydrate Polymers 132 (2015) 481–489

Contents lists available at ScienceDirect

Carbohydrate Polymers

journal homepage: www.elsevier.com/locate/carbpol

Investigation of physical and biological properties of polypyrrole nanotubes–chitosan nanocomposites

J. Upadhyay[a], A. Kumar[a,*], K. Gupta[b], M. Mandal[b]

[a] Department of Physics, Tezpur University, Napaam, Tezpur 784028, Assam, India
[b] Department of Molecular Biology and Biotechnology, Tezpur University, Napaam, Tezpur 784028, Assam, India

ARTICLE INFO

Article history:
Received 8 February 2015
Received in revised form 12 May 2015
Accepted 8 June 2015
Available online 17 June 2015

Keywords:
PPy-NTs:chitosan nanocomposite
Hydrophilicity
Haemolysis activity
Urease immobilization

ABSTRACT

Polypyrrole nanotubes–chitosan (PPy-NTs:chitosan) nanocomposite films have been synthesized with varying concentration of polypyrrole nanotubes (PPy-NTs) and their physical and biological properties have been investigated. Scanning electron microscopy (SEM) micrographs exhibit the increase in surface roughness of the nanocomposite films with increasing concentration of PPy-NTs. Enhancement in hydrophilicity of the nanocomposite films has been observed after surface functionalization with glutaraldehyde which is attributed to increase in surface energy due to the incorporation of polar groups on the films surface. The increasing amount of PPy-NTs in the nanocomposite leads to an increase in haemolysis activity, while the treatment with glutaraldehyde results in the decrease in haemolysis activity giving rise to higher biocompatibility. Urease immobilization in glutaraldehyde treated films exhibits higher enzymatic activity as compared to that of the untreated films, which is attributed to the enhancement in hydrophilicity and biocompatibility of the PPy-NTs:chitosan nanocomposites after functionalization with glutaraldehyde.

© 2015 Elsevier Ltd. All rights reserved.

1. Introduction

The research on nanomaterials is attracting attention of the researchers worldwide for the development of new materials for applications in different areas like nanobiotechnology, nanoelectronics, sensors, actuators, etc. (Jeong et al., 2014; Luca et al., 2015). Different types of materials such as metals (gold and silver), carbon and polymers (especially conducting polymers) have been used to prepare nanostructured materials such as nanotubes, nanoparticles, nanofibers, etc. which promise a variety of applications including optical and electronic nanodevices as well as biological and chemical sensors (Rajesh & Kumar, 2009). Conducting polymer (PPy, polyaniline, polythiophene, etc.) nanostructures have been widely used for different biological applications because of their ease of synthesis, low toxicity, redox active property, high conductivity and environmental stability (Khomenko, Frackowiak, & Béguin, 2005). In spite of the above-mentioned favourable properties, the poor processibility of conducting polymers remains a key hurdle to their practical applications (Fang et al., 2012). The insolubility of conducting polymers in common solvents also limits their use in biological applications (Cabuk, Alan, Yavuz, & Unal, 2014). However, dispersion of low dimensional conducting polymers such as nanotubes, nanoparticles, nanofibers, etc. in different matrices offers the possibility of improving the processibility of these polymers.

Recently, biopolymers such as chitosan, cellulose etc. have been considered for the dispersion of different nanostructured materials, for instance conducting polymer based nanomaterials, carbon nanotubes, metal and metal oxide nanoparticles because of their excellent film-forming ability (Dutta, Tripathi, Mehrotra, & Dutta, 2009). Chitosan possesses remarkable properties like biocompatibility, biodegradability, non-toxicity, hydrophilicity, biofunctionality, etc. which make chitosan as a meritorious host for biological applications (No, Meyers, Prinyawiwatkul, & Xu, 2007; Yan, Wang, Wu, Li, & Ding, 2014). Excellent biocompatibility of chitosan favours an effective immobilization of biomolecules on its surface. In addition, chitosan has reactive amino and hydroxyl groups and can be modified chemically to alter its properties that enhance the functionality of chitosan. On the other hand, to improve the different properties like mechanical strength, electrical conductivity and bioactivity of chitosan membranes, dispersion of different nanostructured materials within the chitosan have been considered. The dispersion of nanomaterials within chitosan enhances the bio-adhesion and can also promote electron transfer

* Corresponding author. Tel.: +91 3712275553; fax: +91 3712267006.
E-mail address: ask@tezu.ernet.in (A. Kumar).

http://dx.doi.org/10.1016/j.carbpol.2015.06.028
0144-8617/© 2015 Elsevier Ltd. All rights reserved.

kinetics and improve the sensitivity and stability of the biosensors (Anusha et al., 2014). Recently a number of PPy–chitosan composites have been reported by different groups. Huang et al. (2013) investigated electrical and swelling properties of PPy–chitosan composite hydrogels. In another work, Lee, Temmer, Tamm, Aabloo, and Kiefer (2013) reported renewable antioxidant property of PPy–chitosan composites. The effect of electrical stimulation on the growth of olfactory ensheathing cells has been investigated by Qi et al. (2013) using PPy–chitosan composite. Though composites of bulk PPy with chitosan have been reported by different groups, there are only few reports on nanocomposites of chitosan with PPy nanostructures. In the present work, we have reported polypyrrole nanotubes:chitosan (PPy-NTs:chitosan) nanocomposites for urease immobilization. Moreover, enhancement in enzyme immobilization as well as biocompatibility of the nanocomposites film after surface functionalization with glutaraldehyde has been investigated in terms of the degree of hydrophilicity of the films.

PPy-NTs:chitosan nanocomposites have been synthesized by dispersing PPy-NTs in chitosan matrix. PPy-NTs were synthesized via methyl orange–ferric chloride (MO–$FeCl_3$) reactive self degrade template method. Different amounts of PPy-NTs viz., 0.5, 2, 4 and 6 wt.% with respect to chitosan are dispersed in the chitosan matrix, which results in PPy-NTs:chitosan nanocomposite films. The structural property, thermal stability and wettability of the nanocomposite films with varying PPy-NTs concentration have been investigated using different characterization tools. Biocompatibility and urease immobilization activity of the nanocomposite films have also been investigated.

2. Experimental

2.1. Materials

Monomer (pyrrole, Sigma Aldrich) was vacuum dried prior to use. Methyl orange (MO) and ferric chloride ($FeCl_3$) from Sisco Research Laboratory (SRL) were used as received. Chitosan (degree of deacetylation (DDA) 90%) was received from SRL.

2.2. Synthesis

2.2.1. Synthesis of polypyrrole nanotubes

PPy-NTs were synthesized via reactive self-degrade MO–$FeCl_3$ template method. In a typical procedure 0.243 g (1.5 m mol) of $FeCl_3$ was dissolved in 30 mL of 5 mM methyl orange (MO) deionised water (0.15 m mol). The appearance of flocculent precipitate was observed instantly. 105 μL (1.5 m mol) of pyrrole was added to the reaction solution. The solution appeared black after a little while indicating the polymerization of pyrrole. The mixture was stirred at room temperature for 24 h to complete the polymerization. The precipitate was washed with deionized water and ethanol several times until the filtrate became colourless and was separated by centrifugation. PPy-NTs, thus formed, were dried in a desiccator overnight.

2.2.2. Synthesis of polypyrrole nanotubes (PPy-NTs):chitosan nanocomposites

The prepared PPy-NTs were subsequently used to synthesis PPy-NTs:chitosan nanocomposite films. For this purpose chitosan solution was prepared by dissolving it in 2 vol.% acetic acid solution by ultrasonication. PPy-NTs powder with varying concentration such as 0.5, 2, 4 and 6 wt.% with respect to chitosan were dispersed in chitosan solution by ultrasonication. The nanocomposite solution was subsequently cast on glass slides and allowed to dry for 48 h at room temperature giving PPy-NTs:chitosan nanocomposite films.

2.3. Analysis and characterization techniques

The surface morphology of pure chitosan as well as nanocomposite films was investigated using scanning electron microscope (SEM) model JEOL JSM 6390 LV at 15–20 kV accelerating voltage. The nanotubular structure of PPy was confirmed by high resolution transmission electron microscopy (HRTEM) studies with a HRTEM model JEOL JEM 2100. X-ray diffractograms were recorded by Rigaku miniflex X-ray diffractometer with 5°/min scan rate. The FTIR spectra were accomplished using a Nicolet Impact 410 spectrometer in the range of 500–4000 cm^{-1}. Thermogravimetric analysis (TGA) was carried out by using a Perkin Elmer, model STA 6000 thermal analyzer with a dynamic nitrogen flow of 20 ml min^{-1}. Contact angle measurements were performed using contact angle measurement system from Data physics instrument GmbH, Germany, model OCA 15 EC at room temperature using three different liquids including, two polar liquids: water and ethylene glycol and one non-polar liquid:diiodomethane. The biocompatibility of pure chitosan and nanocomposite films was investigated by haemolysis assay. For this purpose mammalian red blood cells (RBC) were used and the haemolysis caused by different samples was recorded using spectroscopic technique. Immobilization of enzyme (urease) on the nanocomposite films was performed through physical adsorption method. For immobilization of urease each film was cut in the size of 1.5 cm × 1 cm and one set of films was treated with glutaraldehyde and a comparative study was performed over the immobilized enzyme activity before and after functionalization with glutaraldehyde.

2.4. Haemolysis assay

The haemolytic activity assay was performed according to the method described by Das et al. (2014) with slight modification. Fresh mammalian blood was collected in a centrifuge tube containing anticoagulant trisodium citrate (4%), and was centrifuged at 3000 rpm for 20 min at 4 °C. The supernatant was discarded and only the RBCs or erythrocytes were collected. RBCs were further washed thrice with phosphate buffer saline (PBS, pH 7.4). A 5% (v/v) suspension of erythrocytes in PBS was prepared, and 1.9 mL of this erythrocyte solution was placed in a 2 mL centrifuge tube and 2 mg of each sample was placed in the corresponding tubes. The tubes were incubated for 1–3 h at 37 °C. Triton X-100 and PBS were taken as positive and negative controls, respectively. After incubation, the tubes were subjected to centrifugation at 3500 rpm for 5 min. The absorbance of the supernatant was taken at 540 nm in the UV–visible spectrophotometer.

2.5. Urease immobilization assay

Immobilization of urease on PPy-NTs:chitosan nanocomposite films with 4 wt.% of PPy-NTs of 1.5 cm × 1 cm size was performed by physical adsorption method. For this purpose one set of nanocomposite films was treated with 2 vol.% of glutaraldehyde solution. Urease solution was prepared in 1 mL of phosphate buffer solution (pH 7.4) by dissolving 1 mg of urease (activity 370 unit/mg). Subsequently the films were treated with 200 μL urease solution and stored for 24 h at 4 °C. Urease encapsulated films were then washed with phosphate buffer solution. The activity of the immobilized urease was determined using Nessler's method. UV–vis absorption at 470 nm was measured to determine the activity of the immobilized urease.

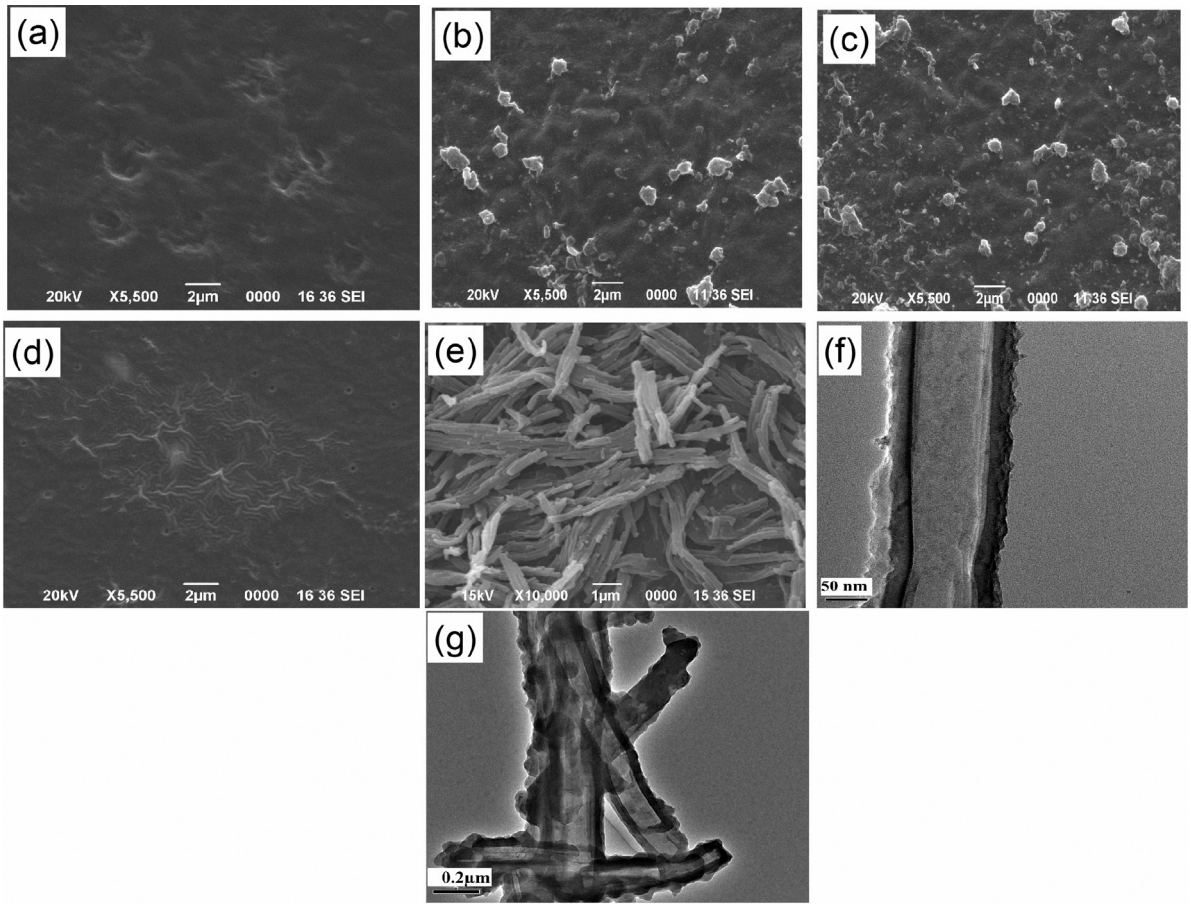

Fig. 1. SEM micrographs of (a) pure chitosan, PPy-NTs:chitosan nanocomposites with (b) 0.5 wt.%, (c) 4 wt.%, (d) 6 wt.% of PPy-NTs, (e) SEM image of PPy-NTs and HRTEM image of (f) PPy-NTs and (g) PPy-NTs:chitosan nanocomposite.

3. Results and discussion

3.1. Electron microscopy analysis

The morphology of pure chitosan and PPy-NTs:chitosan nanocomposites with varying PPy-NTs concentration examined by SEM is displayed in Fig. 1. The SEM images depict the change in surface morphology before and after incorporation of PPy-NTs into the chitosan matrix. From the Fig. 1(a) it is observed that pure chitosan exhibits smooth and porous morphology. The surface roughness of the nanocomposite films increases significantly on incorporation of PPy-NTs into the chitosan matrix as shown in Fig. 1(b) and (c). For 6 wt.% concentration aggregation of PPy-NTs takes place as observed in Fig. 1(d). SEM and HRTEM images of pure PPy-NTs are presented in Fig. 1(e) and (f), respectively. Dispersion of PPy-NTs in the chitosan matrix as observed by HRTEM is presented in Fig. 1(g). The average outer diameter of PPy-NTs has been measured to be about 178 nm from the HRTEM images (Fig. 1(f) and (g)).

3.2. X-ray diffraction study

Fig. 2(i) depicts the X-ray diffraction (XRD) patterns of pure chitosan and PPy-NTs:chitosan nanocomposites with varying concentration of PPy-NTs. It is noticed that pure chitosan exhibits characteristic broad peak located at $2\theta = 22.5^\circ$ which is an evidence of semicrystalline property of the biopolymer [12]. PPy-NTs:chitosan nanocomposites also exhibit diffraction peak in the 2θ range of 15°–35° but the peak intensity decreases on increasing PPy-NTs concentration signifying the increase in amorphicity in the nanocomposites. These results reveal that the incorporation of PPy-NTs affects the crystallinity of nanocomposites and the nanocomposites acquire a heterogeneous structure consisting of amorphous and crystalline domains. The relative crystallinity percentage (X_c) of the nanocomposite films has been calculated using Eq. (1) by measuring the amorphous area and the area of crystalline peak.

$$X_c = \left[\frac{A_c}{A_c + A_a}\right] \times 100 \quad (1)$$

where, A_c is the area of the crystalline domain and A_a is the area of the amorphous region. It is observed that the % crystallinity of the nanocomposites decreases with increase in PPy-NTs concentration. The relative crystallinity of pure chitosan and nanocomposite films with 0.5, 2, 4 and 6 wt.% of PPy-NTs are calculated to be 28.11, 26.27, 25.60, 23.01 and 22.86, respectively.

3.3. FTIR spectroscopy

Fig. 2(ii) exhibits FTIR spectra for pure chitosan and PPy-NTs:chitosan nanocomposites. The bands appearing at 1026 and 1154 cm^{-1} corresponds to C—O—C and C—O linkage of chitosan, respectively (Pawlak & Mucha, 2003). Strong band at 1415 cm^{-1} is ascribed to the CH_2 bending (scissoring) vibration (Liu, Thormann, Claesson, & Tyrode, 2014). In the absorption spectra of pure chitosan the absorption band at 1630 cm^{-1} reflects the vibration of C=O stretching of secondary amide while shoulder peak at 1584 cm^{-1} corresponds to the N—H bending of $-NH_2$ (Wan, Xu, Sun, & Li, 2013; Yang, Tu, Li, Shang, & Tao, 2010). The shifting of C=O bond stretching vibration to the lower wavenumber at 1622 cm^{-1}

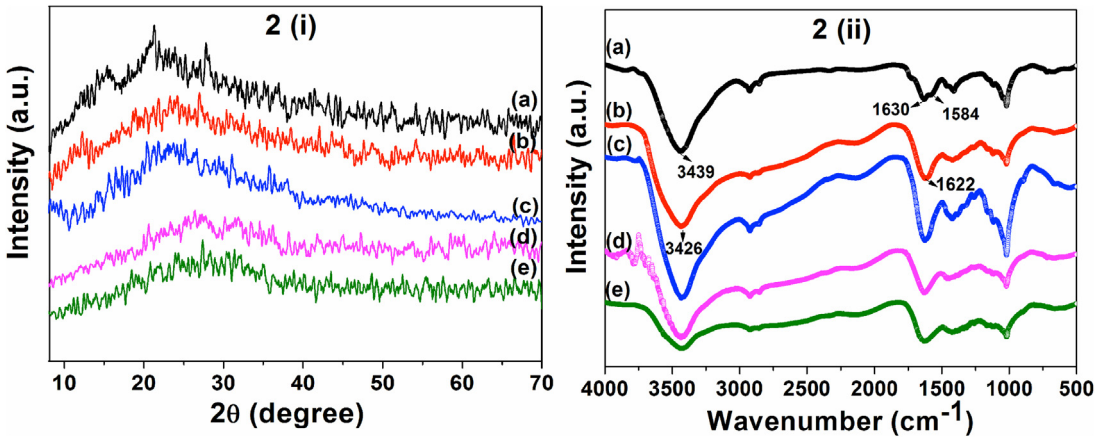

Fig. 2. (i) X-ray diffractograms and (ii) FTIR spectra of (a) pure chitosan, and PPy-NTs:chitosan nanocomposites with (b) 0.5 wt.%, (c) 2 wt.%, (d) 4 wt.% and (e) 6 wt.% of PPy-NTs.

in the nanocomposites suggests the formation of hydrogen bond between the secondary amide group of chitosan and —NH group of PPy-NTs (Li, Xia, & Li, 2012). Moreover, the disappearance of the shoulder peak at 1584 cm^{-1} in nanocomposites indicates the superposition of N—H bending vibration of secondary amine group of PPy and primary amine group of chitosan resulting in the overlapping of the band with the C=O stretch of secondary amide at 1622 cm^{-1} (Shang, Zeng, & Tao, 2012). The signals related to CH and CH_2 stretching appear at 2856 and 2927 cm^{-1}, respectively (Pires et al., 2013). The broad band of pure chitosan centred at 3439 cm^{-1} is assigned to the O—H stretching, which overlaps with the N—H stretching in the same region (Pires et al., 2013). It is observed that the 3439 cm^{-1} band shifted to 3426 cm^{-1} when PPy-NTs were incorporated in the chitosan matrix, which is attributed to the electrostatic interaction between —OH functional groups of chitosan and —NH group of PPy-NTs (Shang, Gan, & Yuen, 2013). PPy-NTs exhibit characteristic bands in the region of 1557 and 1465 cm^{-1} due to C=C and C—N stretching vibration, respectively (Chaohe, Sun, & Gao, 2011). The disappearance of distinct characteristics absorption band of PPy-NTs in the FTIR spectra of the nanocomposites is attributed to the overlapping of 1557 and 1465 cm^{-1} bands of PPy with the 1641 and 1415 cm^{-1} bands of chitosan, respectively.

3.4. Thermal stability study

Thermal stability of the nanocomposites has been studied by thermogravimetric analyzer and the results are depicted in Fig. 3(i). Different slope in the thermograms indicates a distinct degradation mechanism. It is observed from the plot that pure chitosan exhibits slightly higher thermal stability as compared to that of the nanocomposites and with increase in PPy-NTs concentration in the nanocomposite the thermal stability decreases which is attributed to the decrease in crystallinity of the nanocomposite as revealed by the X-ray diffractogram. It is also evident from the thermograms that pure chitosan and PPy-NTs:chitosan nanocomposites exhibit two-step thermal degradation. The first decomposition slope around 90 °C corresponds to the evaporation of adsorbed water in the system. The second degradation slope between 190 and 390 °C is attributed to the decomposition of both chitosan and PPy-NTs (Guo et al., 2015). In this temperature range the degradation of side bonds and backbone of both chitosan and PPy takes place (Guo et al., 2015; Upadhyay & Kumar, 2014).

The derivative plot of the TG plots is presented in the Fig. 3(ii) which exhibits two peaks for both pure chitosan and the nanocomposites corresponding to two different degradation mechanisms. In the case of second degradation mechanism for pure chitosan, T_{onset} = 200 °C and T_{rpd} = 317 °C and from T_{onset} to T_{rpd} around 24% of weight loss takes place. In the case of the nanocomposite having 6 wt.% of PPy-NTs, T_{onset} = 190 °C, T_{rpd} = 296 °C and about 19% of weight loss has been recorded between T_{onset} to T_{rpd}. It is observed that with the increase in amount of PPy-NTs in the nanocomposites, both T_{rpd} and degradation rate decrease continuously. In addition, the decrease in degradation rate from T_{onset} to T_{rpd} with increasing PPy-NTs concentration is attributed to the suppression of thermally degraded components of the nanocomposites by the PPy-NTs. PPy-NTs act as mass transport barrier to the volatile species that are produced during the degradation process, which results in the

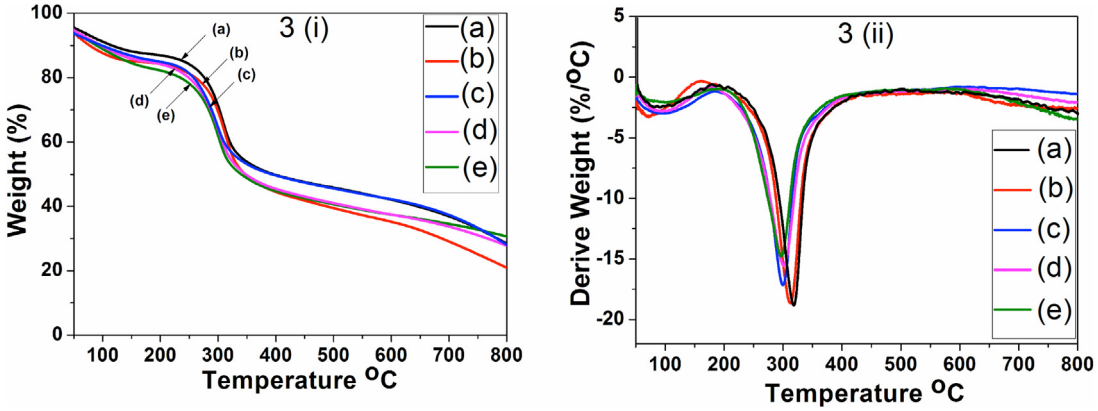

Fig. 3. (i) TG plots and (ii) derivative TG plots of (a) pure chitosan and PPy-NTs:chitosan nanocomposites with (b) 0.5 wt.%, (c) 2 wt.%, (d) 4 wt.% and (e) 6 wt.% of PPy-NTs.

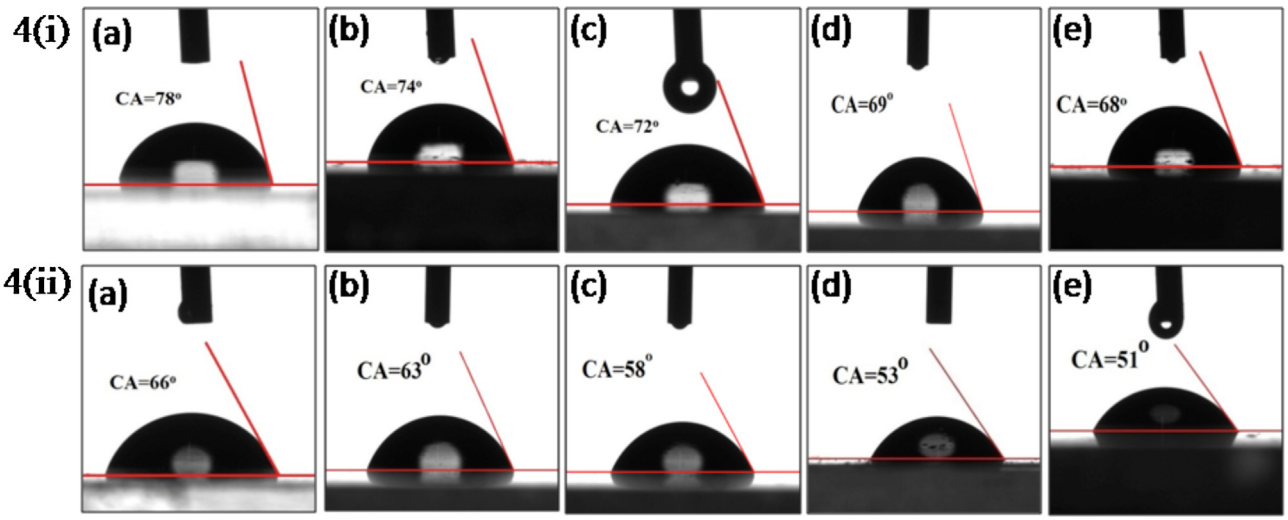

Fig. 4. Water contact angles (i) before and (ii) after glutaraldehyde treatment of (a) pure chitosan and PPy-NTs:chitosan nanocomposites with (b) 0.5 wt.%, (c) 2 wt.%, (d) 4 wt.% and (e) 6 wt.% of PPy-NTs.

decrease in degradation rate with increasing in PPy-NTs concentration in the nanocomposites.

3.5. Contact angle measurement

The surface and interfacial properties of materials are very important for biomedical applications as they influence phenomena such as wettability, adhesion and adsorption. Contact angle is a characteristic parameter that determines the interaction between a liquid and solid. The surface wettability is closely related to the surface free energy and is governed by two factors (i) chemical composition and (ii) roughness of the surface (Sheng, Jiyang, & Tsao, 2007). Water contact angle measurements on pure chitosan and PPy-NTs:chitosan nanocomposite films have been presented in Fig. 4. Pure chitosan membrane is hydrophilic with a contact angle of 78° (Fig. 4i (a)). The incorporation of PPy-NTs in the chitosan matrix results in the decrease in contact angle to 68° for 6 wt.% of PPy-NTs (Fig. 4i (e)). The increased wettability of the nanocomposites with increase in PPy-NTs concentration can be explained on the basis of Wenzel assumption (Yang, Hsu, Chang, Kuo, & Chen, 2010). Wenzel predicts that the wettability of a surface depends on the surface roughness and the contact angle at a surface is given as,

$$\cos\theta_a = r\cos\theta_o \tag{2}$$

where r is surface roughness factor and is defined as the ratio of rough surface area to total surface area, θ_a is the apparent contact angle measured at the geometric level of rough surface and θ_o is the contact angle on a smooth surface. It is observed from the SEM images that the surface roughness of the nanocomposite films increases with increase in PPy-NTs concentration that leads to increase in the surface roughness factor r resulting in the decrease in the contact angle.

The films have been treated with glutaraldehyde in order to enhance the hydrophilicity. The contact angles of water, diiodomethane and ethylene glycol for glutaraldehyde treated and untreated films are presented in the Table 1. It is observed that the water contact angles of both pure and nanocomposite films reduce significantly after treating with glutaraldehyde (Fig. 4(ii)). It should be noted that glutaraldehyde contains functional groups such as —CHO and —OH that can form hydrogen bonds with water molecules, which renders the surface treated with glutaraldehyde more hydrophilic than that of the untreated surface (Sung, Chen, Huang, Hsu, & Chang, 2000). To confirm the enhancement of surface hydrophilicity of the glutaraldehyde treated films, we have calculated the surface energy by using contact angles of three different liquids, two polar liquids: water and ethylene glycol, and one apolar liquid:diiodomethane.

To confirm the modification of glutaraldehyde treated samples we have employed Lifshitz–van der Waals/acid–base (AB) theory for free surface energy evaluation whose outputs with reference to diiodomethane, ethylene glycol, and deionized water as wetting liquids (Chibowski & Perea-Carpio, 2002). According to this theory, the surface tension consists of into two components (i) polar and (ii) apolar components,

$$\gamma_i^{total} = \gamma_i^{LW} + \gamma_i^{AB} \tag{3}$$

where γ_i^{total}, γ_i^{LW} and γ_i^{AB} refer to total energy, apolar (Lifshitz–van der waals) and polar (acid–base) components of surface tension, respectively. γ_i^{AB} can be expressed as:

$$\gamma_i^{AB} = 2(\gamma_S^- \gamma_S^+)^{\frac{1}{2}} \tag{4}$$

where γ_s^+ and γ_s^- indicate the ion pair acceptor (Lewis acid) and the ion pair donor (Lewis base) contributions, respectively.

The results obtained from Lifshitz–van der Waals/acid–base theory are presented in Table 2. It is observed that the nanocomposite films exhibit very small acid component as compared to the basic component. Moreover, significant enhancement in the total energy γ_s^{total} is observed after functionalization with glutaraldehyde, which is assisted by the polar component rather than the apolar one signifying the incorporation of polar groups on the nanocomposites film surface due to functionalization with glutaraldehyde. The contact angle of water decreases as the surface free energy on the glutaraldehyde treated surface increases, indicating the improved wettability of the surface. The percentage of

Table 1
Contact angles of water, ethylene glycol and diiodomethane with pure chitosan and PPy-NTs:chitosan nanocomposites before and after glutaraldehyde treatment.

Sample	Water		Ethylene Glycol		Diiodomethane	
	Before	After	Before	After	Before	After
Chitosan	78°	66°	65°	52°	57°	55°
0.5 wt.%	74°	63°	61°	50°	55°	53°
2 wt.%	72°	58°	59°	45°	54°	51°
4 wt.%	69°	53°	57°	42°	55°	52°
6 wt.%	68°	51°	56°	35°	52°	49°

Table 2
Values of γ^+, γ^-, γ_S^{LW}, γ_S^{total} and percentage of polarity calculated by using AB method for pure chitosan and nanocomposite films before and after glutaraldehyde treatment.

Sample	γ^+	γ^-	γ_S^{LW}	γ_S^{total} (mN m^{-1})	Polarity (%)
Before					
Chitosan	0.01	13.08	30.31	31.19	2.67
0.5 wt.%	0.00	16.13	31.44	31.44	1.5
2 wt.%	0.00	17.06	32.01	32.01	2.01
4 wt.%	0.01	20.5	31.44	32.34	2.8
6 wt.%	0.00	20.96	33.15	33.15	3.5
After					
Chitosan	0.10	24.87	31.44	34.59	8.9
0.5 wt.%	0.08	24.38	32.65	35.44	7.87
2 wt.%	0.11	28.36	33.38	37.38	9.63
4 wt.%	0.16	33.98	33.15	37.81	12.3
6 wt.%	0.33	32.7	34.9	41.49	15.8

polar component has been calculated by using the Eq. (5) and is presented in Table 2:

$$\text{polarity}\,(\%) = \frac{\gamma_S^{AB}}{\gamma_S^{Total}} \times 100 \tag{5}$$

The improvement in the polarity after functionalization with glutaraldehyde is attributed to the interaction of glutaraldehyde with free amino groups of PPy-NTs and chitosan that gives rise to in the incorporation of functional groups such as —CHO and —OH on the nanocomposite films. This increased polarity enhances the adsorption in the glutaraldehyde modified surface due to of its better wettability, which is useful for biomedical applications.

To further confirm the incorporation of polar groups on the surface of the glutaraldehyde treated films, the Owens, Wendt, Rabel and Kaelble (OWRK) method has been used for the calculation of the total surface energy in terms of polar and dispersive parts (López-Pérez, Marques, da Silva, Pashkuleva, & Reis, 2007). This method is based on the contact angles measurements of two liquids, one polar (ethylene glycol) and other apolar (diiodomethane). The polar component of the surface tension is the estimation of concentration of polar groups that are present on the surface. Slight variation has been observed in the total energy values calculated by the two methods, though both the methods exhibit similar trends in the total energy values (data by OWRK method are not presented here). In both the methods, also the enhancement of surface energy of the glutaraldehyde treated films is assisted by the polar component rather than by the dispersive part.

3.6. Haemolysis activity

Materials intended for biomedical applications require their characterization by haemocompatibility, also known as blood compatibility. Haemocompatibility of a material depends on material blood interaction and control by the properties of both the material and the blood. The haemocompatibility of pure chitosan and PPy-NTs:chitosan nanocomposites has been carried out with mammalian RBC through haemolysis assay. Haemolysis is destruction of RBC either by chemical or mechanical stress to an erythrocyte that causes the release of haemoglobin in the surrounding media and can be readily quantified using spectrophotometry (Khan, Kapoor, & Kumar, 2007). Haemolysis activity is measured by measuring the optical density at 540 nm using an ultraviolet spectrophotometer and the percentage of haemolysis is calculated using the following formula:

$$\%\text{Haemolysis} = \frac{OD_{sample} - OD_{negative\ control}}{OD_{positive\ control} - OD_{negative\ control}} \times 100 \tag{6}$$

Triton X-100 has been used as positive control and the haemolysis induced by it is considered as 100% haemolysis. Phosphate buffer (PBS) has been used as negative control corresponding to no destruction of RBC. The percent haemolysis for different samples before and after functionalization with glutaraldehyde has been calculated by using Eq. (6) has been presented in Fig. 5(a). All the experiments were repeated twice to ensure uniform results and the standard deviation (SD) is calculated by using the Eq. (7).

$$\text{SD} = \sqrt{\left[\frac{1}{(N-1)}\sum_{i=1}^{N}(x_i - \bar{x})^2\right]} \tag{7}$$

where, $x_1, x_2, \ldots, x_i$ are the observed values of the absorbance, $\bar{x}$ is the mean value of these observations and N is the number of times the experiments were conducted. To investigate the haemolysis activity of pure and nanocomposite films, equal quantity of 2 mg of each membrane was treated with RBC. It is observed that pure chitosan exhibits haemolysis around 1.28%. Chitosan is considered a good biocompatible material for different biomedical applications but lacks haemocompatibility. The haemolysis activity of chitosan is attributed to the interaction of free amino groups of chitosan with the blood cells leading to the rupturing of RBCs and is attributed in part to the electrostatic interaction (Balan & Verestiuc, 2014). In addition, the incorporation of PPy-NTs in the chitosan film results in the increase in haemolysis activity, which is attributed to the cytotoxic effects of PPy-NTs. Conducting PPy is considered as low toxic material in biological media and the toxicity increases with increasing PPy concentration. Moreover, the increased surface roughness of the nanocomposite films with increase in PPy-NTs concentrations may also induce haemolysis by destroying the surface of blood cells (Khan et al., 2007). It is observed that films treated with glutaraldehyde exhibit less haemolysis activity than that of the corresponding untreated films. This enhancement in biocompatibility of the glutaraldehyde treated films is attributed to the increase in hydrophilicity of the films due to incorporation of polar groups on the film surface. SEM images of pure chitosan and PPy-NTs:chitosan nanocomposite films with 4 wt.% of PPy-NTs before and after RBC treatment (1 h incubation time) have been presented in Figs. 1(a, c) and 5 (b, c), respectively. It is seen that the deformation of RBC is more in case of nanocomposite films than that of pure chitosan, which is evidence of increased haemolysis activity of the nanocomposite films. An increase in haemolysis activity is observed with the increase of sample incubation time from 1 h to 3 h.

3.7. Activity of immobilized urease

The activity of the free and immobilized urease has been investigated through hydrolysis of urea that gives rise to the production of ammonia and can be detected by spectroscopic method. The relative activity of the conjugated urease is predicted through the determination of ammonia concentration by Nessler's method. Upon exposure of the urease immobilized film to urea, an enzymatic reaction takes place that can be represented as

$$NH_2CONH_2 + 2H_2O \rightarrow 2NH_4^+ + CO_3^{2-} \tag{8}$$

The produced ammonia reacts with Nessler's reagent to form a coloured product and is detected spectroscopically by an absorption peak at 470 nm which is proportional to the ammonia concentration. The relative activity of the immobilized urease with time has been determined by comparing the activity of free urease and is presented in Fig. 6(i). It is observed that films treated with glutaraldehyde exhibit higher enzymatic activity than that of the untreated films. 72.1% of the urease immobilized in the glutaraldehyde treated films retain their activity, whereas 49.2% of

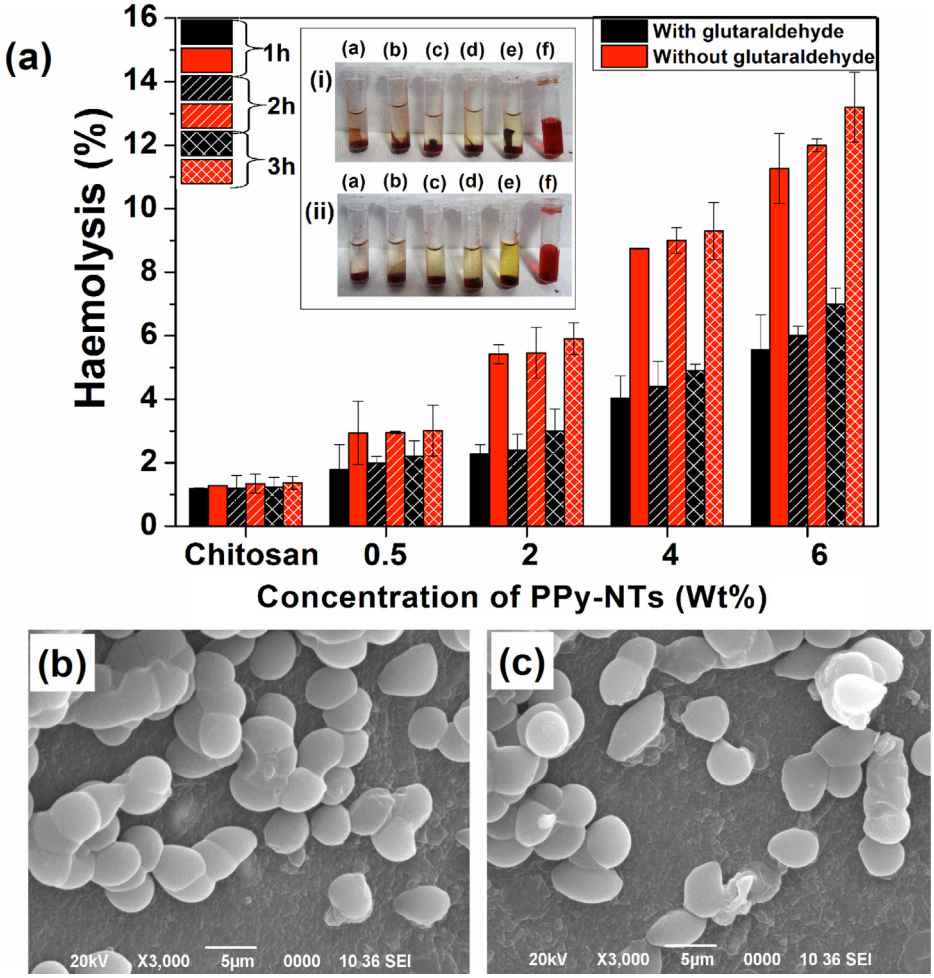

Fig. 5. (a) Percentage haemolysis by pure chitosan and PPy-NTs:chitosan nanocomposites before and after glutaraldehyde treatment presented in the form of mean value ± standard deviation as a function of incubation time. Inset photographs of RBC treated with 2 mg of each sample (i) before, and (ii) after glutaraldehyde treatment of (a) pure chitosan, and PPy-NTs:chitosan nanocomposites with (b) 0.5 wt.%, (c) 2 wt.%, (d) 4 wt.%, (e) 6 wt.% of PPy-NTs and (f) triton X-100. SEM images showing morphology of the RBCs with (b) pure chitosan and (c) PPy-NTs:chitosan nanocomposite with 4 wt. % of PPy-NTs.

the immobilized urease preserve their activity in the untreated films after 10 min of reaction time. The enhanced enzymatic activity of the glutaraldehyde treated films is attributed to the increased hydrophilicity and biocompatibility of the films. The increased hydrophilicity of the glutaraldehyde treated films assists the enzyme adsorption on the films surface leading to enhanced enzymatic activity. Moreover, glutaraldehyde may act as a cross-linker between the nanocomposite, film and urease that enhances the enzyme attachment on the film surface leading to higher enzymatic activity of the glutaraldehyde treated films.

The Michaelis constant is determined from the Lineweaver–Burk plot as shown in Fig. 6(ii). The activity of both free and immobilized urease has been determined in 0.01 M phosphate buffer saline (pH 7.4). The graph is plotted taking different concentrations of substrate and their corresponding reaction rate. The reciprocal of substrate concentration ($1/S$) is

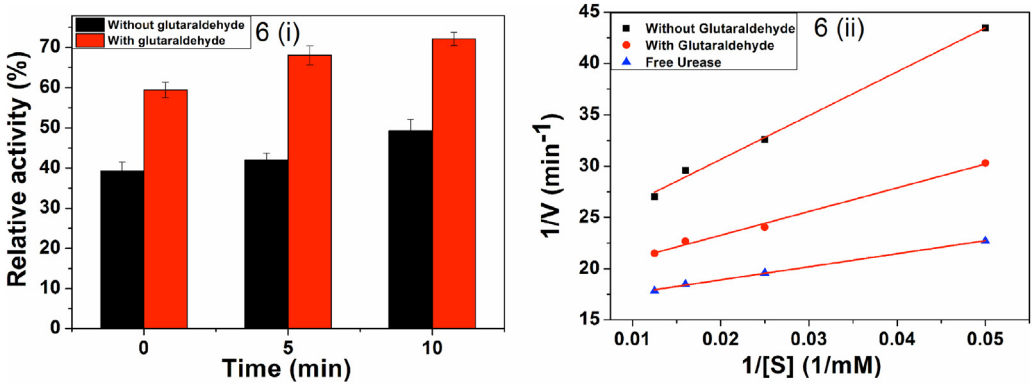

Fig. 6. (i) Relative activity of immobilized urease with time on glutaraldehyde treated and untreated films, and (ii) Lineweaver–Burk plot of free and immobilized urease.

plotted against the reciprocal of the reaction rate ($1/V$) according to the following equation,

$$\frac{1}{V} = \frac{K_m}{V_{max}} \frac{1}{[S]} + \frac{1}{V_{max}} \quad (9)$$

From the Fig. 6(ii) it is observed that both free and immobilized enzyme exhibit linear Lineweaver–Burk plot obeying Michaelis–Menten enzyme kinetics. The intercept of the straight line gives the value of inverse of maximum hydrolysis rate ($1/V_{max}$) of urea, whereas the slope gives the ratio of Michaelis constant to the maximum hydrolysis rate (K_m/V_{max}). Ideally lower K_m is preferred as it represents a high biocatalytic activity (Bayramoğlu, Yalçin, & Arica, 2005). From the Lineweaver–Burk plot we have obtained the values of K_m to be 7.78 mM, 12.24 mM and 19.19 mM for free urease, glutaraldehyde treated and untreated films, respectively. The K_m of the immobilized enzyme is different from that of the free enzyme due to diffusion limitations of substrate (urea) in the pore space of the support (PPy-NTs:chitosan nanocomposite) (Bayramoğlu et al., 2005). The small K_m value of the glutaraldehyde treated film than that of the untreated film is attributed to the fact that the glutaraldehyde treated film can immobilize the enzyme at high load/activity because of its enhanced hydrophilicity (Crespilho, Lost, Travain, Oliveiria, & Zucolotto, 2009).

4. Conclusions

PPy-NTs:chitosan nanocomposites have been synthesized by dispersing pre-synthesized PPy-NTs in chitosan matrix through ultrasonication. SEM micrographs exhibit increase in surface roughness of the nanocomposite films with increasing concentration of PPy-NTs. The average outer diameter of PPy-NTs is measured to be 178 nm by HRTEM. In FTIR spectra, the shifting of the C=O stretching vibration of pure chitosan at 1630 cm^{-1} to 1622 cm^{-1} in the nanocomposites suggests the formation of hydrogen bond between the secondary amide group of chitosan and —NH group of PPy-NTs. Thermal studies depict a decrease in T_{onset}, T_{rpd} and percentage of weight loss between T_{onset} to T_{rpd} with the increase in concentration of PPy-NTs in the nanocomposites. PPy-NTs act as mass transport barrier to the thermally degraded components of the nanocomposite, which results in the decrease in degradation rate from T_{onset} to T_{rpd} with increasing concentration of PPy-NTs in the nanocomposite. The decrease in the contact angle of the nanocomposite films with increasing PPy-NTs concentration is attributed to the increase in surface roughness of nanocomposite films, which is consistent with the Wenzel prediction. The glutaraldehyde treated films exhibit lower contact angle value as compared to that of the untreated films that is attributed to the incorporation of polar groups —OH and —CHO on the film surface. The increased hydrophilicity of the glutaraldehyde treated films is confirmed by calculating surface energy of the films using OWRK and AB methods. On increasing the amount of PPy-NTs the haemolysis activity of the nanocomposites increases due to the increased cytotoxicity of PPy-NTs towards RBC. The treatment with glutaraldehyde renders the nanocomposite films more biocompatible as compared to the untreated films. Glutaraldehyde treated films show higher enzymatic activity that may be attributed to the increased hydrophilicity and biocompatibility of the films. Glutaraldehyde may also acts as cross-linker, interconnecting urease and nanocomposite film, giving rise to higher enzymatic activity.

References

Anusha, J. R., Kim, H.-J., Fleming, A. T., Das, S. J., Yu, K.-H., Kim, B. C., et al. (2014). Simple fabrication of ZnO/Pt/chitosan electrode for enzymatic glucose biosensor. *Sensors and Actuators B*, *202*, 827–833.

Balan, V., & Verestiuc, L. (2014). Strategies to improve chitosan haemocompatibility: A review. *European Polymer Journal*, *53*, 171–188.

Bayramoğlu, G., Yalçin, E. M., & Arıca, Y. (2005). Immobilization of urease via adsorption onto L-histidine-Ni(II) complexed poly(HEMA-MAH) microspheres: Preparation and characterization. *Process Biochemistry*, *40*, 3505–3513.

Cabuk, M., Alan, Y., Yavuz, M., & Unal, H. I. (2014). Synthesis, characterization and antimicrobial activity of biodegradable conducting polypyrrole-graft-chitosan copolymer. *Applied Surface Science*, *318*, 168–175.

Chaohe, X., Sun, J., & Gao, L. (2011). Synthesis of novel hierarchical graphene/polypyrrole nanosheet composites and their superior electrochemical performance. *Journal of Materials Chemistry*, *21*, 11253–11258.

Chibowski, E., & Perea-Carpio, R. (2002). Problems of contact angle and solid surface free energy determination. *Advances in Colloid and Interface Science*, *98*, 245–264.

Crespilho, F. N., Iost, R. M., Travain, S. A., Oliveiria, O. N., Jr., & Zucolotto, V. (2009). Enzyme immobilization on Ag nanoparticles/polyaniline nanocomposites. *Biosensors and Bioelectronics*, *24*, 3073–3077.

Das, P. M., Manhar, A. K., Das, V. K., Borah, A., Mandal, M., Thakur, A. J., et al. (2014). Antioxidative, haemocompatible, fluorescent carbon nanodots from an end-of-pipe agricultural waste: Exploring its new horizon in the food-packaging domain. *Journal of Agricultural Food Chemistry*, *62*, 4509–4520.

Dutta, P. K., Tripathi, S., Mehrotra, G. K., & Dutta, J. (2009). Perspectives for chitosan based antimicrobial films in food applications. *Food Chemistry*, *114*, 1173–1182.

Fang, Y., Ni, Y., Zhang, G., Mao, C., Huang, X., & Shen, J. (2012). Biocompatibility of CS-PPy nanocomposites and their application to glucose biosensor. *Bioelectrochemistry*, *88*, 1–7.

Guo, M., Ma, Y., Wang, C., Liu, H., Li, Q., & Fei, M. (2015). Synthesis, anti-oxidant activity, and biodegradability of a novel recombinant polysaccharide derived from chitosan and lactose. *Carbohydrate Polymers*, *118*, 218–223.

Huang, H., Wu, J., Lin, X., Li, L., Shang, S., Yuen, M. C.-W., et al. (2013). Self-assembly of polypyrrole/chitosan composite hydrogels. *Carbohydrate Polymers*, *95*, 72–76.

Jeong, H.-H., Mark, A. G., Gibbs, J. G., Reindl, T., Waizmann, U., Weis, J., et al. (2014). Shape control in wafer-based aperiodic 3D nanostructures. *Nanotechnology*, *25*, 235302, 7 pp.

Khan, W., Kapoor, M., & Kumar, N. (2007). Covalent attachment of proteins to functionalized polypyrrole-coated metallic surfaces for improved biocompatibility. *Acta Biomaterialia*, *3*, 541–549.

Khomenko, V., Frackowiak, E., & Béguin, F. (2005). Determination of the specific capacitance of conducting polymer/nanotubes composite electrodes using different cell configurations. *Electrochimica Acta*, *50*, 2499–2506.

Lee, R.-J., Temmer, R., Tamm, T., Aabloo, A., & Kiefer, R. (2013). Renewable antioxidant properties of suspensible chitosan–polypyrrole composites. *Reactive & Functional Polymers*, *73*, 1072–1077.

Li, L., Xia, K., & Li, L. (2012). Fabrication and characterization of free-standing polypyrrole/graphene oxide nanocomposite paper. *Journal of Nanoparticle Research*, *14*, 908.

Liu, C., Thormann, E., Claesson, P. M., & Tyrode, E. (2014). Surface grafted chitosan gels. Part I. Molecular insight into the formation of chitosan and poly(acrylic acid) multilayers. *Langmuir*, *30*, 8866–8877.

López-Pérez, P. M., Marques, A. P., da Silva, R. M. P., Pashkuleva, I., & Reis, R. L. (2007). Effect of chitosan membrane surface modification via plasma induced polymerization on the adhesion of osteoblast-like cells. *Journal of Materials Chemistry*, *17*, 4064–4071.

Luca, M. D., Zilli, A., Fonseka, H. A., Mokkapati, S., Miriametro, A., Tan, H. H., et al. (2015). Polarized light absorption in wurtzite InP nanowire ensembles. *Nano Letters*, http://dx.doi.org/10.1021/nl5038374

No, H. K., Meyers, S. P., Prinyawiwatkul, W., & Xu, Z. (2007). Applications of chitosan for improvement of quality and shelf life of foods: A review. *Journal of Food Science*, *72*, 87–100.

Pawlak, A., & Mucha, M. (2003). Thermogravimetric and FTIR studies of chitosan blends. *Thermochimica Acta*, *396*, 153–166.

Pires, N. R., Cunha, P. L. R., Maciel, J. S., Angelim, A. L., Melo, V. M. M., de Paula, R. C. M., et al. (2013). Sulfated chitosan as tear substitute with no antimicrobial activity. *Carbohydrate Polymers*, *91*, 92–99.

Qi, F., Wang, Y., Ma, T., Zhu, S., Zeng, W., Hu, X., et al. (2013). Electrical regulation of olfactory ensheathing cells using conductive polypyrrole/chitosan polymers. *Biomaterials*, *34*, 1799–1809.

Rajesh, T. A., & Kumar, D. (2009). Recent progress in the development of nano-structured conducting polymers/nanocomposites for sensor applications. *Sensors and Actuators B*, *136*, 275–286.

Shang, S., Gan, L., & Yuen, M. C.-W. (2013). Improvement of carbon nanotubes dispersion by chitosan salt and its application in silicone rubber. *Composites Science and Technology*, *86*, 129–134.

Shang, S., Zeng, W., & Tao, X.-M. (2012). Fabrication of conducting polypyrrole/b-cyclodextrin nano- and microsphere using molecular templates. *RSC Advances*, *2*, 4675–4682.

Sheng, Y.-J., Jiang, S., & Tsao, H.-K. (2007). Effects of geometrical characteristics of surface roughness on droplet wetting. *Journal of Chemical Physics*, *127*, 234704–234707.

Sung, H.-W., Chen, C.-N., Huang, R.-N., Hsu, J.-C., & Chang, W.-H. (2000). In vitro surface characterization of a biological patch fixed with a naturally occurring cross-linking agent. *Biomaterials*, *21*, 135–1362.

Upadhyay, J., & Kumar, A. (2014). Investigation of structural, thermal and dielectric properties of polypyrrole nanotubes tailoring with silver nanoparticles. *Composite Science Technology*, *97*, 55–62.

Wan, A., Xu, Q., Sun, Y., & Li, H. (2013). Antioxidant activity of high molecular weight chitosan and N,O-quaternized chitosans. *Journal of Agricultural Food Chemistry*, *61*, 6921–6928.

Yan, J., Wang, H., Wu, T., Li, X., & Ding, Z. (2014). Elastic and electrically conductive carbon nanotubes/chitosan composites with lamellar structure. *Composites: Part A*, *67*, 1–7.

Yang, X., Tu, Y., Li, L., Shang, S., & Tao, X.-M. (2010). Well-dispersed chitosan/graphene oxide nanocomposites. *Applied Materials and Interfaces*, *2*, 1707–1713.

Yang, Y.-L., Hsu, C.-C., Chang, T.-L., Kuo, L.-S., & Chen, P.-H. (2010). Study on wetting properties of periodical nanopatterns by a combinative technique of photolithography and laser interference lithography. *Applied Surface Science*, *256*, 3683–3687.